Repurposing propofol for breast cancer therapy through promoting apoptosis and arresting cell cycle

PENG SUN[1*], HANQING HUANG[2*], JIAN-CHAO MA[2*], BINYANG FENG[2], YIQING ZHANG[2], GENGGENG QIN[3], WEIAN ZENG[1] and ZHONG-KAI CUI[2]

[1]Department of Anesthesiology, State Key Laboratory of Oncology in South China, Guangdong Provincial Clinical Research Center for Cancer, Sun Yat-sen University Cancer Center, Guangzhou, Guangdong 510060, P.R. China; [2]Department of Cell Biology, School of Basic Medical Sciences, Southern Medical University, Guangzhou, Guangdong 510515, P.R. China; [3]Department of Radiology, Nanfang Hospital, Southern Medical University, Guangzhou, Guangdong 510515, P.R. China

Received February 23, 2024; Accepted June 17, 2024

DOI: 10.3892/or.2024.8814

Abstract. Breast cancer is the most prevalent cancer among women worldwide, characterized by a high mortality rate and propensity for metastasis. Although surgery is the standard treatment for breast cancer, there is still no effective method to inhibit tumor metastasis and improve the prognosis of patients with breast cancer after surgery. Propofol, one of the most widely used intravenous anesthetics in surgery, has exhibited a positive association with improved survival outcomes in patients with breast cancer post-surgery. However, the underlying molecular mechanism remains to be elucidated. The present study revealed that triple negative breast cancer cells, MDA-MB-231 and 4T1, exposed to propofol exhibited a significant decrease in cell viability. Notably, propofol exhibited minimal cytotoxic effects on HUVECs under the same conditions. Furthermore, propofol significantly inhibited the migration and invasion ability of MDA-MB-231 and 4T1 cells. Propofol promoted apoptosis in 4T1 cells through upregulation of Bax and cleaved caspase 3, while downregulating B-cell lymphoma-extra large. Concomitantly, propofol induced cell cycle arrest of 4T1 cells by downregulating cyclin E2 and phosphorylated cell division cycle 6. Furthermore, propofol exhibited excellent anticancer efficacy in a 4T1 breast cancer allograft mouse model. The present study sheds light on the potential of propofol as an old medicine with a novel use for breast cancer treatment.

Correspondence to: Professor Weian Zeng, Department of Anesthesiology, State Key Laboratory of Oncology in South China, Guangdong Provincial Clinical Research Center for Cancer, Sun Yat-sen University Cancer Center, 74 Zhongshan 2nd Road, Yuexiu, Guangzhou, Guangdong 510060, P.R. China
E-mail: zengwa@sysucc.org.cn

Professor Zhong-Kai Cui, Department of Cell Biology, School of Basic Medical Sciences, Southern Medical University, S. 1023 Shatai Road, Guangzhou, Guangdong 510515, P.R. China
E-mail: zhongkaicui@smu.edu.cn

*Contributed equally

Key words: propofol, apoptosis, cell cycle arrest, repurposed drug, triple-negative breast cancer

Introduction

Breast cancer remains a formidable global health challenge, with its prevalence and impact on life expectancy underscoring the pressing demand for innovative therapeutic strategies (1). In 2019 alone, breast cancer accounted for 30% of newly diagnosed malignancies and 15% of fatalities among women (2). As one of the most prevalent malignancies affecting women, breast cancer imposes a significant burden on both healthcare systems and societal well-being (3). The complexities of breast cancer encompass not only its diverse molecular subtypes, including the notoriously aggressive triple-negative breast cancer, but also its propensity for tumor growth, metastasis and the emergence of therapeutic resistance (4-6).

Contemporary breast cancer treatments primarily include surgical resection, chemotherapy, radiotherapy, endocrine therapy, immunotherapy and targeted therapy. The strategies for breast cancer management vary across stages (7,8). While surgical removal combined with preoperative endocrine therapy or chemotherapy offers a potential cure for early-stage and non-metastatic locally advanced-stage cases, palliative care becomes the primary recourse for metastatic patients, aiming to extend and enhance the quality of life (4,9,10). Surgical resection is a favored option, especially for patients with early-stage disease. However, the perioperative period, characterized by the activation of neural and inflammatory signaling pathways, which can disrupt immune function and affect cancer progression, has been associated with increased metastatic potential (11,12). The choice of anesthetics during breast cancer surgery has been demonstrated to influence patient outcomes and the risk of postoperative recurrence (13,14).

The exploration of repurposed drugs as potential candidates for cancer treatment has gained considerable momentum (15,16). This paradigm shift capitalizes on the existing pharmacopeia to identify novel applications for established drugs, thereby expediting the development of effective

therapies (17,18). Among these repurposed agents, propofol, a longstanding intravenous anesthetic renowned for its sedative properties, has emerged as an intriguing candidate in the field of oncology (19). While traditionally valued for its anesthetic attributes, propofol has begun to unveil an unexpected facet of its pharmacological profile-a capacity to modulate tumor biology (20-22).

Preclinical investigations have revealed its potential to exert antitumor effects across diverse cancer types (23-25). Clinical observations have indicated that the use of propofol as an anesthetic is associated with reduced breast cancer metastasis compared with alternative agents (14,26). Retrospective clinical analyses comparing propofol with sevoflurane, an alternative anesthetic, have demonstrated that the former is associated with improved survival, with the latter associated with heightened endoplasmic reticulum stress in tumor and immune cells, thereby impacting prognosis (26-28). Preliminary research underscores the inhibitory effect of propofol on tumor cell proliferation, apoptosis induction and metastasis; however, the intricate mechanisms remain elusive (29,30). Despite these advancements, controversies persist regarding its antitumor effects on breast cancer, with a number of studies suggesting its potential to promote the migration of breast cancer cells and divergent findings on its impact on apoptosis mechanisms (31,32). Therefore, unraveling its function in breast cancer cells and elucidating its inhibitory mechanisms holds profound clinical significance.

The present study aimed to elucidate the antitumor effects of propofol, specifically on triple-negative breast cancer, both *in vitro* and *in vivo*. Triple-negative breast cancer currently lacks effective clinical treatments compared with the estrogen receptor (ER)-, progesterone receptor- and/or HER-2-positive subtypes. The investigations of the present study encompassed a comprehensive assessment, ranging from inhibiting tumor growth to inducing apoptosis and modulating cell cycle progression. Through this multifaceted exploration, the present study aimed to reveal the potential of repurposing propofol as an innovative therapeutic avenue in triple-negative breast cancer treatment. Delving into the intricate interplay between propofol and tumor biology, the present findings hold the promise of steering the course towards novel and impactful therapeutic strategies.

Materials and methods

Materials. Propofol was supplied by Shanghai Macklin Biochemical Co., Ltd., while the propofol injectable emulsion (10 mg/ml, Diprivan) was purchased from Aspen Pharma Trading Ltd. TRIzol (cat. no. 9109) and the PrimeScript RT reagent kit (cat. no. RR047A) were provided by Takara Bio, Inc. The Whole Cell Lysis Assay (cat. no. KGP250) and BCA Protein quantification assay kit (cat. no. KGP902) were purchased from Nanjing KeyGen Biotech Co., Ltd. SYBR qPCR Master Mix (cat. no. Q341-02) was purchased from Vazyme Biotech Co., Ltd. DMSO (D4540) was obtained from Sigma-Aldrich; Merck KGaA. Methanol, ethanol, xylene, glycerol and Tween-20 were of analytical grade, obtained from Sinopharm Chemical Reagent Co., Ltd., and used without further purification.

Cell culture. Mouse triple-negative breast cancer cells (4T1, cat. no. CRL-2539), human triple-negative breast cancer cells (MDA-MB-231, cat. no. CRM-HTB-26), human umbilical vein endothelial cell line (HUVECs, cat. no. CRL-4053), human chorionic tumor cell line (BeWo, cat. no. CCL-98), human liver cancer cell line (Hep-G2, cat. no. HB-8065) and human cervical cancer cell line (HeLa, cat. no. CCL-13) were procured from the American Type Culture Collection. Human gastric cancer cell line (MKN-45, cat. no. CL-0292), and human endometrial cancer cell line (Ishikawa, cat. no. CL-0283) were procured from Procell Life Science & Technology Co., Ltd. These cells were maintained in growth medium comprising DMEM (Gibco; Thermo Fisher Scientific, Inc.) supplemented with 10% FBS (164210; Procell Life Science & Technology Co., Ltd.) and 1% penicillin/streptomycin (Gibco; Thermo Fisher Scientific, Inc.). Cell cultures were incubated in a humidified atmosphere with 5% CO_2 at 37˚C.

Cell viability assay. Cell viability was determined using a Cell Counting Kit-8 (CCK-8) assay (cat. no. CK04; Dojindo Laboratories, Inc.) according to the manufacturer's protocol. 4T1 cells, MDA-MB-231 cells and HUVECs were seeded in a 96-well cell culture plate at a density of $4x10^3$ cells per well and incubated for 24 h. Subsequently, cells were exposed to varying concentrations (0, 25, 50, 75, 100 and 150 μg/ml; containing 0.1% DMSO) of propofol. After 3, 5 and 7 days of incubation, respectively, fresh medium containing 10 μl CCK-8 reagent was added to each well. Following a 1-h incubation in the dark at 37˚C, the absorbance at 450 nm was measured using a microplate reader (SynergyHTX; Agilent Technologies, Inc.). The normalized relative cell viability was calculated as follows: Relative cell viability=$(A_s-A_b)/(A_c-A_b)$ x100%, where A_b, A_c and A_s are the absorbance intensities of the blank, the positive control and the sample, respectively.

Wound healing assay. For the wound healing assay, 4T1 cells, MDA-MB-231 cells and HUVECs were cultured in 24-well plates and allowed to adhere overnight to form a monolayer, respectively. Subsequently, a uniform scratch was created in the cell monolayer, and a sterile PBS solution was used to remove any cellular debris. The cells were then exposed to culture medium (DMEM without FBS or PS) supplemented with varying concentrations (0, 50 and 100 μg/ml; containing 0.1% DMSO) of propofol for 24 h. Images of the scratched areas were captured at both the initial time point (0 h) and after 24 h of treatment using a Nikon Eclipse TE2000-U microscope (Nikon Corporation). This approach allowed for the observation and quantification of cell migration and closure of the scratch over the designated time period. The average width of the scratched gap was measured in triplicate wells using the ImageJ software (v.1.6.0; National Institutes of Health).

Transwell assay. The Transwell migration assay was employed to meticulously evaluate the effect of propofol on cell migration. 4T1 cells, MDA-MB-231 cells and HUVECs were seeded in the Falco™ chamber with 8-μm pores (Corning, Inc.) at a density of $5x10^4$ cells per well. Ensuring precision, the outer chamber membrane was scrupulously cleaned post-cell adhesion to eliminate non-specific attached cells. Subsequently, media containing varying concentrations (0, 50 and 100 μg/ml;

containing 0.1% DMSO) of propofol were introduced into the respective chambers. The wells of the corresponding 24-well plates were simultaneously loaded with basal growth medium (DMEM with 10% FBS and 1% PS). Following an incubation period of 24 h at 37˚C, the chambers underwent a gentle wash with PBS before fixation with 4% paraformaldehyde for 30 min at room temperature. The migration assessment ensured through the application of 0.1% crystal violet staining (cat. no. G1064; Beijing Solarbio Science & Technology Co., Ltd.) to the cells that had successfully traversed the membrane for 20 min at room temperature, while non-migratory cells remaining atop the membranes were removed. Images of migratory cells were captured using an inverted microscope (Eclipse TE2000-U; Nikon Corporation). ImageJ software (v.1.6.0; National Institutes of Health) was used to analyze the data.

RNA sequencing (RNA-seq) of the 4T1 cell transcriptome. 4T1 cells were exposed to growth media containing varying concentrations (0 and 100 μg/ml; containing 0.1% DMSO) of propofol. Following a 12-h incubation period at 37˚C, cell lysis was performed using TRIzol reagent to extract total RNA according to the manufacturer's instructions. Then RNA quality was determined by 5300 Bioanalyser (Agilent Technologies, Inc.) and quantified using the ND-2000 (NanoDrop Technologies; Thermo Fisher Scientific, Inc.). Only high-quality RNA samples (OD 260/280=1.8~2.2, OD 260/230 ≥2.0, RIN ≥6.5, 28S:18S ≥1.0, >1 μg) was used to construct sequencing library. The RNA-seq transcriptome library was prepared following Illumina® Stranded mRNA Prep, Ligation (Illumina, Inc.) using 1 μg of total RNA. Messenger RNA was isolated according to polyA selection method by oligo(dT) beads and then fragmented by fragmentation buffer firstly. Secondly double-stranded cDNA was synthesized using a SuperScript double-stranded cDNA synthesis kit (Invitrogen; Thermo Fisher Scientific, Inc.) with random hexamer primers (Illumina, Inc.). Then, the synthesized cDNA was subjected to end-repair, phosphorylation and 'A' base addition according to Illumina's library construction protocol. Libraries were size selected for cDNA target fragments of 300 bp on 2% Low Range Ultra Agarose followed by PCR amplified using Phusion DNA polymerase (NEB) for 15 PCR cycles. After quantification by Qubit 4.0, paired-end RNA-seq sequencing library was sequenced with the NovaSeq 6000 sequencer (2x150 bp read length). Significance analysis was performed using both P-value and false discovery rate (FDR) analysis. Genes exhibiting differential expression were identified based on fold change criteria, where fold changes >2 or <0.5 and an FDR <0.05 were considered indicative of differential expression. Pathway analysis, referencing the Kyoto Encyclopedia of Genes and Genomes (KEGG; https://www.genome.jp/kegg/pathway.html) database, was employed to discern significantly influenced pathways associated with the identified differentially expressed genes.

Apoptosis induction assay. 4T1 cells were seeded in a 12-well plate at a density of $8x10^4$ cells per well. After 24 h of incubation at 37˚C, the cells were subjected to distinct concentrations (0 and 100 μg/ml; containing 0.1% DMSO) of propofol, incorporated within basal growth media. After incubation for 12 h at 37˚C, cells were systematically stained using an annexin V-FITC apoptosis analysis kit (cat. no. AO2001-02P-H; Tianjin Sungene Biotech Co., Ltd.) in accordance with the manufacturer's protocol. The cells were subsequently digested using 0.25% trypsin and the resulting cell suspension was centrifuged for 4 min at 180 x g at 4˚C, yielding a cell precipitate. After resuspension in PBS, the annexin V-positive cell population was separated using a flow cytometer (CytoFLEX; Beckman Coulter, Inc.), and the resulting data were analyzed using CytExpert (V2.0; Beckman Coulter, Inc.).

Cell cycle analysis. 4T1 cells were seeded in a 12-well plate at a density of $8x10^4$ cells per well. After 24 h of incubation at 37˚C, the cells were subjected to distinct concentrations (0 and 100 μg/ml; containing 0.1% DMSO) of propofol, incorporated within basal growth media. After incubation for 24 h at 37˚C, the cells were digested using 0.25% trypsin, and the resulting cell suspension was centrifuged for 4 min at 180 x g at 4˚C, facilitating the acquisition of a cell precipitate. This cell precipitate was subsequently immersed in 70% pre-cooled ethanol at 4˚C, ensuring a comprehensive fixation overnight. Subsequently, the cells were stained with 0.5 ml of propidium iodide (PI)/RNase Staining Buffer (cat. no. 550825; BD Biosciences) for 15 min at room temperature. The DNA content was assessed utilizing a flow cytometer (CytoFLEX; Beckman Coulter, Inc.), with the excitation wavelength set at 488 nm and emission wavelengths at 585±21 nm. The resultant data were analyzed using CytExpert (V2.0; Beckman Coulter, Inc.).

Western blotting. 4T1 cells were seeded in a 12-well plate at a density of $8x10^4$ cells per well. After incubation for 24 h, the cells were treated with basal media containing distinct concentrations (0 and 100 μg/ml; containing 0.1% DMSO) of propofol. After incubation for 12 h, cellular lysis was performed using the Whole Cell Lysis Assay Kit according to the manufacturer's protocol. Quantification of the protein concentration was performed using the BCA Protein Assay Kit. Equally concentrated samples (10 μg protein loaded per lane) were subjected to electrophoresis in 10% polyacrylamide gels, with subsequent transfer onto nitrocellulose membranes. Membranes were blocked by 5% skim milk in Tris-buffered saline with 0.1% tween 20 (TBST) at room temperature for 1 h. Subsequently, the membranes were cropped, followed by primary antibodies, β-actin (1:10,000; cat. no. RM2001; Beijing Ray Antibody Biotech), B-cell lymphoma-extra large (Bcl-xL; 1:1,000; cat. no. 2764T; Cell Signaling Technology, Inc.), Bax (1:1,000; cat. no. A19684; Abcam), p-CDC6 (1:1,000; cat. no. AP1153; ABclonal Biotech Co., Ltd.), CDC6 (1:1,000; cat. no. 11640-1-AP; Proteintech Group, Inc.), Cyclin E2 (CCNE2; 1:1,000; cat. no. 11935-1-AP; Proteintech Group, Inc.), pro-caspase 3 (1:1,000; cat. no. 14220; Cell Signaling Technology, Inc.) and cleaved caspase 3 (1:1,000; cat. no. A19664; ABclonal Biotech Co., Ltd.) overnight at 4˚C. Afterwards, the membranes underwent triple wash with TBS with Tween-20, followed by incubation with the corresponding secondary antibody (1:3,000; cat. no. RM3002; Beijing Ray Antibody Biotech) at room temperature for 1 h. For signal detection, a chemiluminescent horseradish peroxidase (HRP) substrate kit (cat. no. SQ202; Epizyme, Inc.) was used. The

images were captured using a chemiluminescence system (GeneGnome XRQ; Syngene Europe). The resulting blots were subjected to semi-quantification using ImageJ (v.1.6.0; National Institutes of Health), with normalization against the control group.

Immunofluorescence staining. Cells from distinct treatment groups were fixed with 4% paraformaldehyde for 30 min at room temperature, followed by permeabilization using 0.2% Triton for 15 min. Blocking was performed using goat serum (cat. no. C0265; Beyotime Institute of Biotechnology) for 1 h at 37˚C. After rinsing with PBS, primary antibodies, p-CDC6 (1:200; cat. no. AP1153; ABclonal Biotech Co., Ltd.), Cyclin E2 (CCNE2; 1:200; cat. no. 11935-1-AP; Proteintech Group, Inc.), were applied for incubation overnight at 4˚C. Subsequently, HRP-conjugated secondary antibodies, (1:200), were applied for incubation for 1 h at room temperature. Nuclei were counterstained using 1 μg/ml DAPI (cat. no. D9542; Sigma-Aldrich; Merck KGaA). The cells were then observed under a confocal laser scanning microscope (FV3000; Olympus Corporation). Images were subjected to semi-quantification using ImageJ (v.1.6.0; National Institutes of Health), with normalization against the control group.

Reverse transcription-quantitative PCR (RT-qPCR). Total RNA of cells was extracted using TRIzol reagent. The RNA was subjected to cDNA synthesis using the PrimeScript RT Master Mix (Takara Bio, Inc.) following the manufacturer's protocol. The synthesized cDNA was diluted and subsequently used for RT-qPCR using the SYBR Green Master Mix. The amplification and quantification of target RNA molecules were performed using the CFX96 PCR equipment (Bio-Rad Laboratories, Inc.). The thermocycling protocol consisted of two stages: First stage included 95˚C for 30 sec, with 1 repetition; the second stage involves 95˚C for 10 sec and 60˚C for 30 sec, repeated for 40 cycles. The levels of RNA expression were analyzed using the $2^{-\Delta\Delta Cq}$ method (33), an established approach for relative quantification in qPCR analyses. β-actin was used as a reference control for mRNA. The specific primer sequences used are listed in Table SI.

Xenograft breast tumor model. Female BALB/c mice, aged 8 weeks, weighing ~18-20 g, were utilized in the present study. Ethical clearance for all animal-related procedures was obtained from the Institutional Animal Care and Use Committee of Southern Medical University (Guangzhou, China). The animals were housed under pathogen-free conditions with a 12:12-h light/dark cycle and at a constant temperature (22±2˚C). Furthermore, the mice were given unrestricted access to standard chow and water. The 4T1 tumor xenotransplantation model was selected as the animal model. Cell suspension (100 μl) containing $1x10^6$ 4T1 cells was carefully injected into the second right mammary gland fat pad of female BALB/c mice (n=24). Throughout the experimental period, close monitoring was conducted to assess changes in both body weight and tumor size among the female mice. Tumor volume was calculated using the following equation: V (mm^3)=length x $width^2/2$.

Upon attaining a tumor size of 50 mm^3, the mice were randomly allocated to distinct treatment regimens. Each treatment was administered via intratumoral injection on a daily basis over a span of 14 days. The control group, serving as a comparative benchmark, received injections of 100 μl PBS. Meanwhile, the experimental groups were stratified into concentrations of 10, 40 and 100 mg/ml, each receiving 100 μl of the respective propofol concentration. The largest tumor volume in mice did not exceed 2,000 mm^3. Once tumor volume exceeded 2,000 mm^3, the mice would be euthanized. Tumor volumes of mice were measured once a day. On day 15, mice were euthanized by decapitation under anesthesia. A commercial mouse guillotine (Henan Zhike, Inc.) was used for decapitation of the mice. Prior to this, a 0.3% (60 mg/kg) intraperitoneal injection of pentobarbital sodium was administered. Once the mice were under deep anesthesia, they were humanely sacrificed by decapitation. Tumors as well as major organs were harvested for subsequent experiments.

Histological evaluation. Tumor samples from mice were fixed in 4% paraformaldehyde for 24 h at room temperature. The samples were embedded in paraffin and cut at a thickness of 5 μm. Paraffin sections from tumors and major organs underwent a hematoxylin-eosin staining procedure to elucidate morphological characteristics and molecular markers. Immunohistochemical analysis was performed on tumor tissue sections. Following antigen retrieval using 10 mM citrate buffer (pH 6.0), endogenous peroxidase activity was quenched with 3% hydrogen peroxide solution. To prevent non-specific binding, goat serum (cat. no. C0265; Beyotime Institute of Biotechnology) for 1 h at 37˚C was applied. Primary antibodies, including Bax rabbit monoclonal antibody (mAb) (1:100; 5023T; Cell Signaling Technology, Inc.), Bcl-xL rabbit mAb (1:100; 2764T; Cell Signaling Technology, Inc.) and cleaved caspase 3 rabbit mAb (1:100), were employed for specific target detection by incubation overnight at 4˚C. Subsequent to primary antibody binding, peroxidase-conjugated secondary antibody (1:200) and a DAB kit (cat. no. ZL1-9018; OriGene Technologies, Inc.) were applied to facilitate visualization. Sections were counterstained with hematoxylin. Images were obtained using an upright microscope (Axio Scope A1; Carl Zeiss AG). Images were subjected to semi-quantification using ImageJ (v.1.6.0; National Institutes of Health), with normalization against the control group.

Bioinformatics analysis. Gene Expression Profiling Interactive Analysis 2 (http://gepia2.cancer-pku.cn/#index) was used to assess CCNE2 and cell division cycle 6 (CDC6) expression in different tumors. The Kaplan-Meier plotter (http://www.kmplot.com/), followed by the log-rank test, was utilized to predict the overall survival (OS) and recurrence-free survival (RFS) of patients with breast cancer based on CCNE2 and CDC6 expression from The Cancer Genome Atlas database.

Statistical analysis. Data are presented as the mean ± SD, and were analyzed by the unpaired Student's t-test, one-way ANOVA with Tukey's post hoc test, and two-way ANOVA with Tukey's post hoc test for multiple comparisons using Prism 8 software (GraphPad; Dotmatics). The cell culture experiments were repeated independently at least three times. $P<0.05$ was considered to indicate a statistically significant difference.

Results

Propofol suppresses cell viability in triple-negative breast cancer cells. The *in vitro* cytotoxicity of propofol was evaluated by a CCK-8 assay, revealing dose-dependent and time-dependent inhibition of cell viability in both 4T1 and MDA-MB-231 cells upon exposure to propofol (Fig. 1A and B). On day 3, 4T1 cells exhibited a significant decrease in cell viability when exposed to 75 μg/ml propofol, while as low as 25 μg/ml effectively suppressed their metabolism on days 5 and 7. Similar results were observed for MDA-MB-231 cells. Notably, even at a higher concentration (100 μg/ml) on day 7, propofol exhibited no detectable cytotoxic effect against HUVECs (Fig. 1C). These findings indicated the higher sensitivity of 4T1 and MDA-MB-231 cells to propofol treatment compared with that of HUVECs. Moreover, propofol effectively suppressed cell viability of breast cancer cells, while sparing normal human cells, even at higher concentrations and extended durations. The antitumor effects of propofol were assessed on various cancer cell lines. The findings suggested that the antitumor effects of propofol are not exclusive to breast cancer, instead, it exhibits varying levels of efficacy against different cancer cell types (Fig. S1).

Propofol inhibits cell migration and invasion. The survival of patients with breast cancer is hindered by metastasis. Cell migration is the initial step for cancer metastasis (34,35). To evaluate the effects of propofol on cell migration and invasion, the wound healing assay and Transwell assay were conducted on 4T1 cells, MDA-MB-231 cells and HUVECs. Wound healing progression was recorded at 0 and 24 h, respectively. In all of three cell types, wound healing was notably delayed by propofol, at both 50 and 100 μg/ml, compared with the non-treated control group (Fig. 2). For 4T1 cells, the migration ratio was reduced to ~50% by 50 μg/ml propofol, with no significant difference observed between 50 and 100 μg/ml group (Fig. 2A). Conversely, in MDA-MB-231 cells and HUVECs, propofol had a concentration-dependent effect on migration, with the migration ratio decreasing to <50% in the 100 μg/ml group (Fig. 2B and C).

Cell invasion is a crucial factor contributing to the metastatic dissemination of breast cancer, presenting a formidable obstacle to patient survival. The Transwell assay revealed a dose-dependent effect of propofol, effectively inhibiting cell invasion to varying extents at 24 h (Fig. 3). Notably, 100 μg/ml propofol substantially reduced the invasion ratio of both breast cancer cell lines to <50%. These findings highlight the potential of propofol as a promising therapeutic candidate for mitigating the metastatic behavior of breast cancer cells, and warrant further investigation of its translational implications in enhancing patient outcomes.

Propofol induces cell apoptosis and arrests cell cycle progression. To determine the potential signaling pathways, a comprehensive investigation of global gene expression was conducted using RNA-seq analysis of 4T1 cells, derived from a mouse mammary tumor, which are renowned for their aggressive and metastatic traits. The results exhibited remarkable alterations in gene expression, with 1,354 upregulated genes and 1,186 downregulated genes following propofol treatment (Figs. S2, 4A and B). These findings served as a catalyst for directing the focus towards exploring the impact on apoptosis and cell cycle progression, as revealed through additional KEGG pathway analysis (Fig. 4C). Understanding the regulatory mechanisms governing apoptosis and cell cycle control helps reveal the complexities of tumor development, progression and the formulation of potential treatment strategies.

Flow cytometry was initially employed to investigate the effects of propofol on apoptosis and cell cycle progression in 4T1 cells. The apoptotic rate was increased by a remarkable 25% following treatment with 100 μg/ml propofol (Fig. 5A). Concurrently, propofol treatment led to a significant increase in the proportion of cells in the G_1 phase, accompanied by a reduction in the number of cells in the S phase (Fig. 5B). These findings indicated that propofol effectively induced cell apoptosis and arrested cell proliferation at the G_1 phase, shedding light on its potential as a promising therapeutic agent to regulate both cell apoptosis and cell cycle progression in breast cancer.

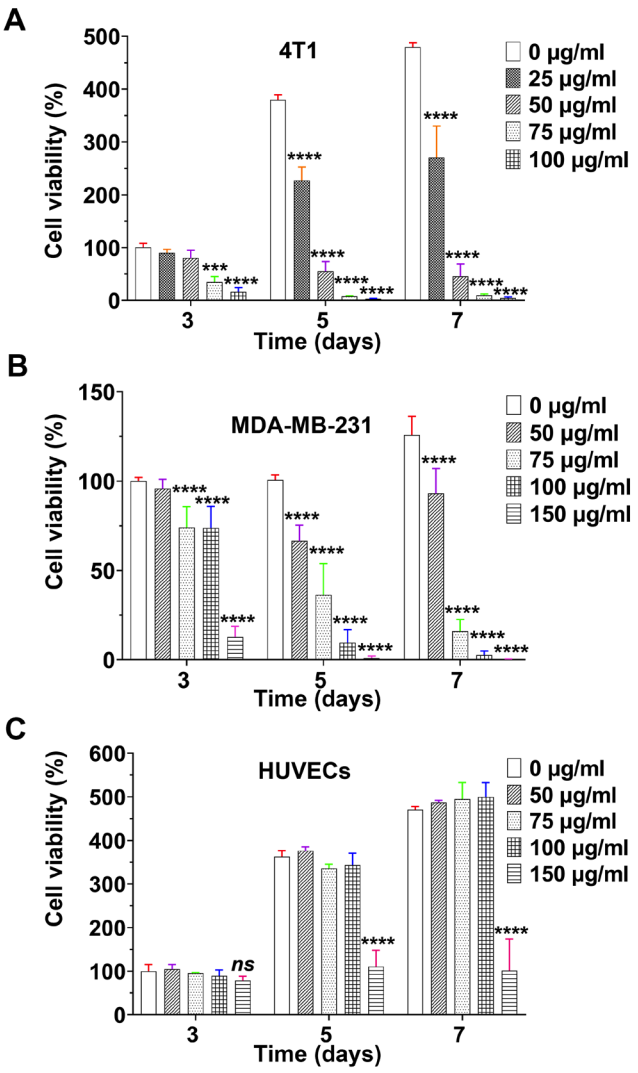

Figure 1. Effects of propofol on cell viability. (A-C) Cell viability of (A) 4T1 cells, (B) MDA-MB-231 cells and (C) HUVECs with varying concentrations of propofol at different time points (n=4). ***P<0.001 and ****P<0.0001. HUVECs, human umbilical vein endothelial cells; ns, no significance.

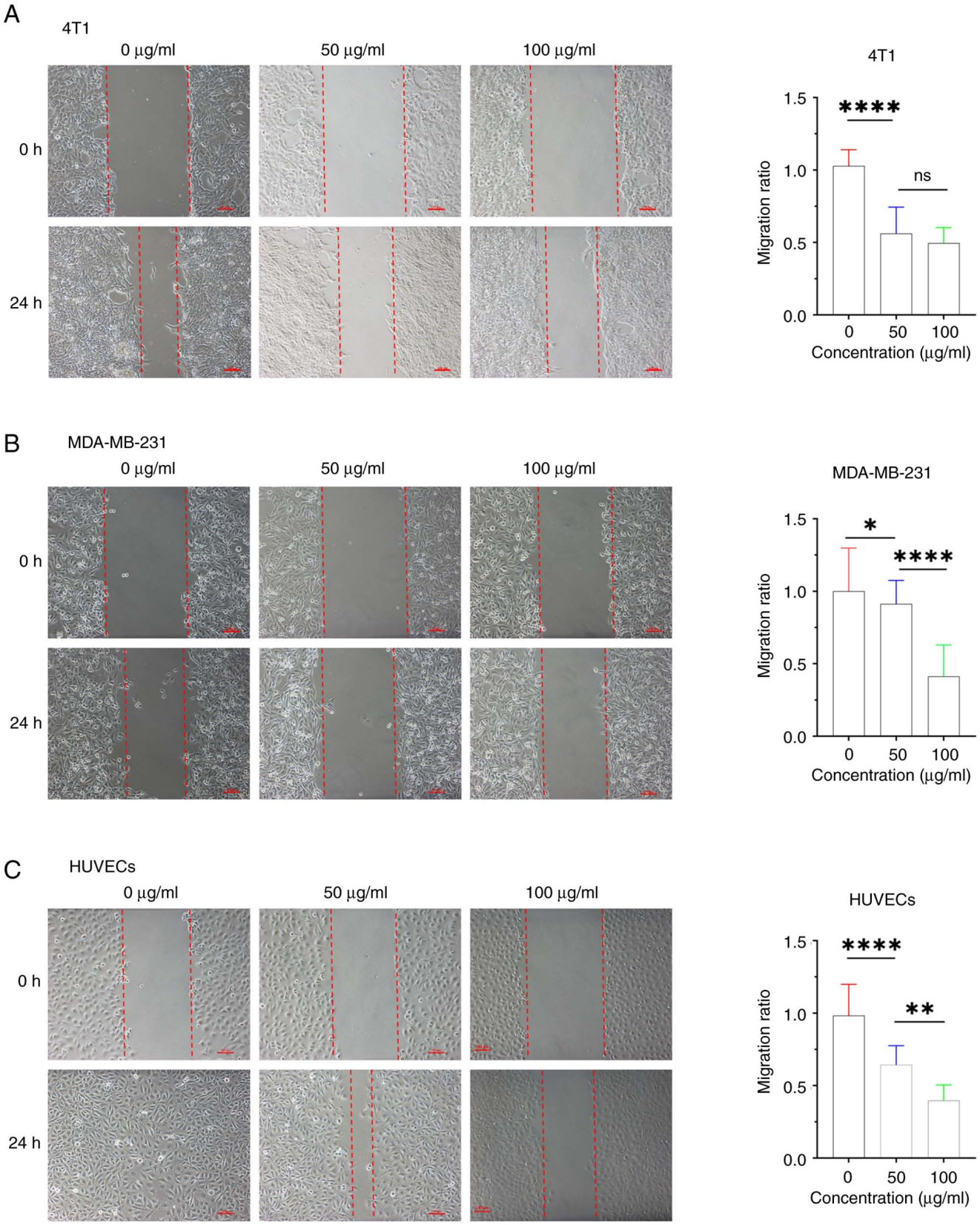

Figure 2. Propofol inhibits cell migration. (A-C) Images and analysis of the migration ratio of the wound-healing assays of (A) 4T1 cells, (B) MDA-MB-231 cells and (C) HUVECs at 0 and 24 h, respectively. Scale bar, 100 μm. Statistical analysis was performed using one-way ANOVA with Tukey's post hoc analysis. Data are presented as the mean ± SD (n=6). *P<0.05, **P<0.01 and ****P<0.0001. HUVECs, human umbilical vein endothelial cells; ns, no significance.

At the molecular level, propofol treatment elicited significant changes in the protein expression of key regulators involved in cell apoptosis and cell cycle progression. Specifically, an increase in the protein expression levels of Bax, an apoptosis agonist marker, and cleaved caspase 3, a crucial indicator of apoptosis activation, was observed following propofol

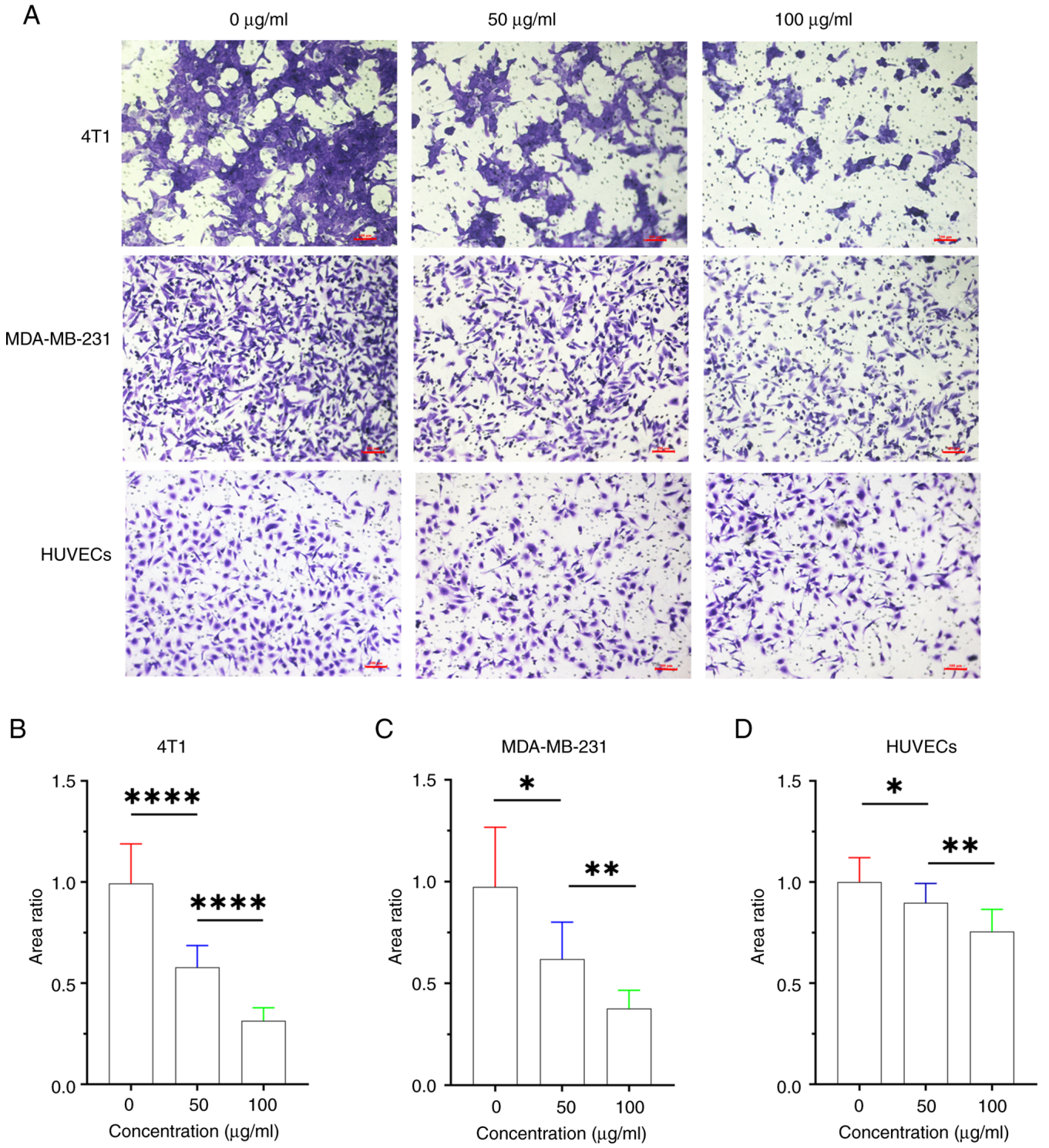

Figure 3. Effects of propofol on cell invasion. (A) Images of the Transwell assays of 4T1 cells, MDA-MB-231 cells and HUVECs at 24 h. Scale bar, 100 μm. (B-D) Analysis of the invasion area ratio for (B) 4T1 cells, (C) MDA-MB-231 cells and (D) HUVECs. Statistical analysis was performed using one-way ANOVA with Tukey's post hoc analysis. Data are presented as the mean ± SD (n=6). *P<0.05, **P<0.01 and ****P<0.0001. HUVECs, human umbilical vein endothelial cells.

treatment (Fig. 6A). Conversely, the expression of Bcl-xL, an apoptosis antagonist marker within the Bcl-2 family, was decreased following propofol treatment, further supporting its pro-apoptotic effects. Regarding cell cycle regulation, the present investigation focused on two pivotal markers, CCNE2 and CDC6, as indicated by the RNA-seq analysis. CCNE2 plays a crucial role in orchestrating the G_1/S transition. Intriguingly, propofol treatment led to a significant decrease in both CCNE2 and phosphorylated CDC6 (p-CDC6) levels, as indicated by western blot analyses and immunofluorescence staining (Fig. 6B and C). This consistent reduction in CCNE2 and CDC6 was further validated at the mRNA level (Fig. 6D), wherein the mRNA expression levels of CCNE2 and CDC6 were significantly downregulated. Specifically, the CCNE2

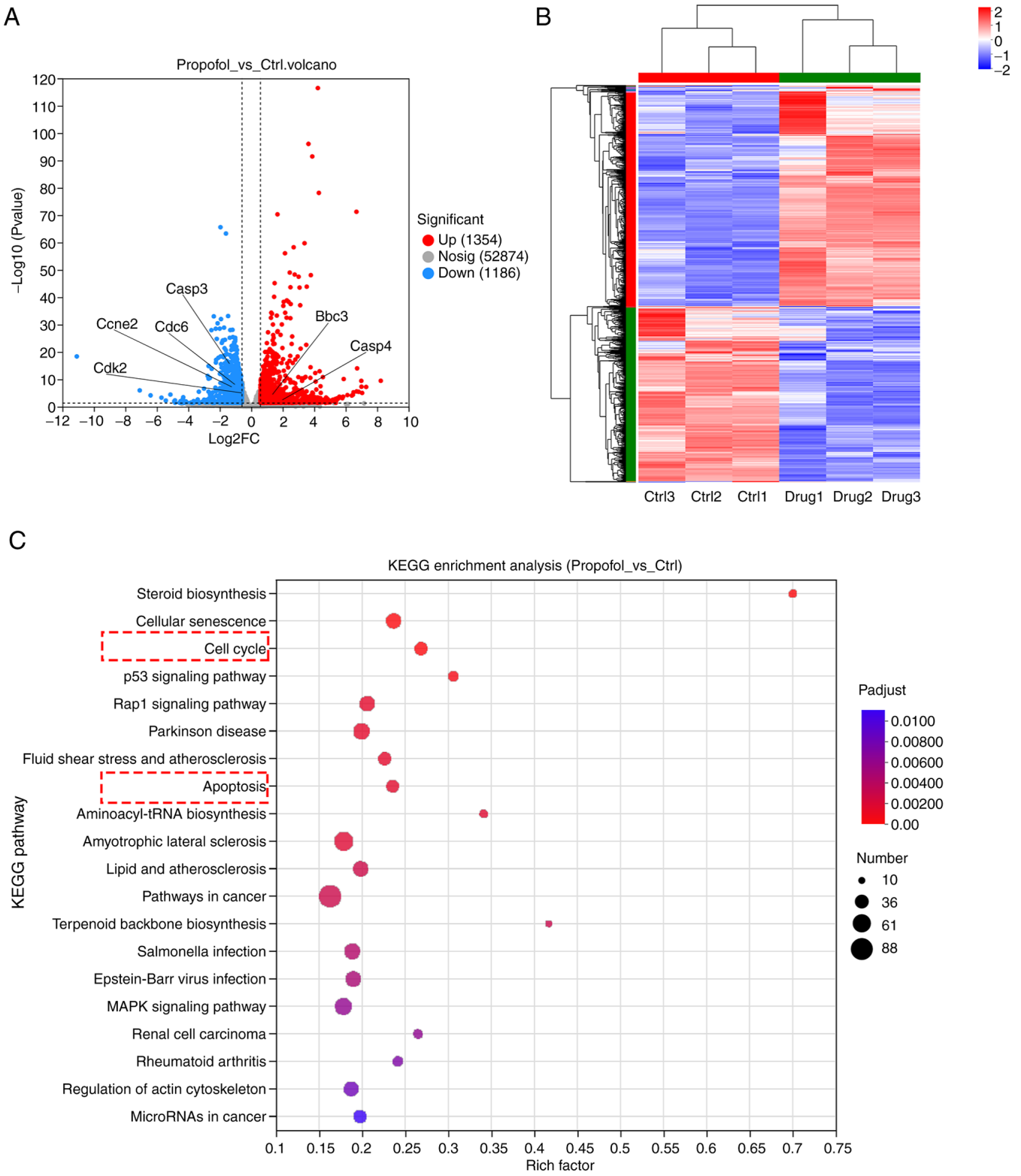

Figure 4. RNA-sequencing analysis of 4T1 cells. (A) Volcano plot depicting gene expression changes between propofol-treated and untreated (Ctrl) groups. Genes with a fold change ≥1.5 and a P-value <0.05 are highlighted in red and blue. (B) Heat map illustrating the differentially expressed genes between the propofol and Ctrl groups. (C) KEGG analysis revealing enriched pathways associated with the differentially expressed genes. KEGG, Kyoto Encyclopedia of Genes and Genomes; Ctrl, control.

mRNA expression was reduced to 43% and the CDC6 mRNA expression was down to 71% compared with the control group, respectively, upon propofol treatment. These findings shed light on the multifaceted impact of propofol treatment on the cell apoptosis and cell cycle progression. The upregulation of pro-apoptotic markers, coupled with the downregulation of antiapoptotic and cell cycle-related factors, further underscores its potential as a promising therapeutic agent in the context of cancer treatment, warranting further exploration in preclinical and clinical settings.

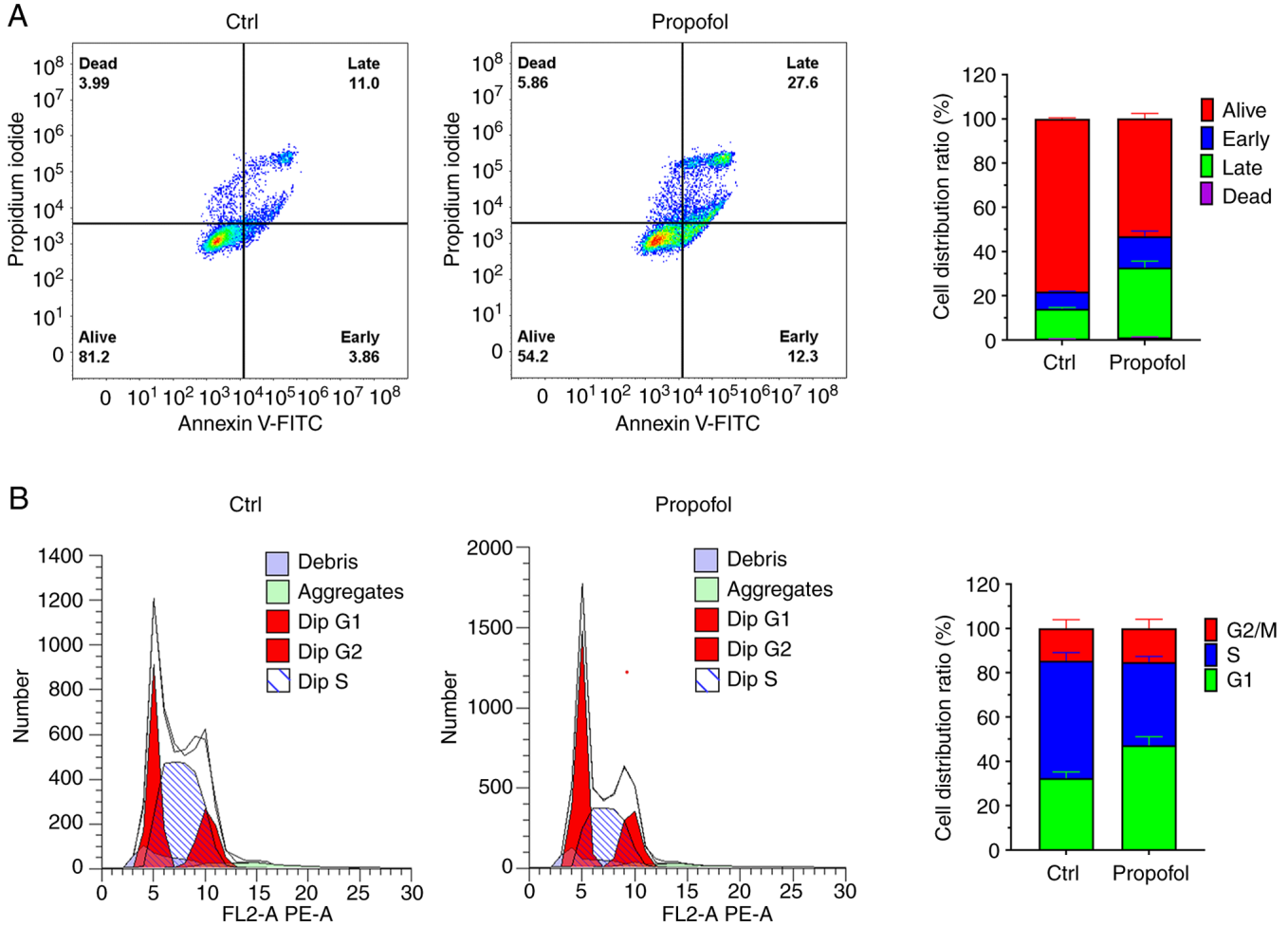

Figure 5. Effects of propofol on cell apoptosis and cell cycle progression. (A) Flow cytometric plots were generated to assess the expression of Annexin V-FITC and PI on 4T1 cell following 24 h treatment with propofol. Quadrants were set based on controls to distinguish positive and negative populations. The histogram displays the quantification of cells in each population. (B) Flow cytometric analysis of 4T1 cells revealed the distribution of cells G_1, S and G_2/M phases following 24 h treatment with propofol. The histogram illustrates the relative proportions of cells in each cell cycle phase. Data are presented as the mean ± SD (n=4). Ctrl, control.

Propofol suppresses tumor growth in vivo. To evaluate the therapeutic potential of propofol *in vivo*, 4T1 tumor-bearing mice were employed and randomly divided into four groups: PBS (control) and propofol at various concentrations (10, 40 and 100 mg/ml). After 14 days of treatment, the mice were euthanized on day 15 and tumor specimens were collected (Fig. 7A). Remarkably, throughout the experimental period, no abnormal changes in the body weight of mice were observed (Fig. S3). These findings further confirmed the excellent biocompatibility of propofol *in vivo* at high concentrations, highlighting its potential for safe clinical application.

The efficacy of each treatment was assessed by monitoring tumor volume evolution and the dissected tumor volume (Fig. 7B and C). For the *in vivo* animal experiments, a total of 24 mice were euthanized after anesthesia on the designated endpoint day 14, with no tumor volume exceeding 2,000 mm^3. Groups treated with PBS and 10 mg/ml propofol exhibited minimal tumor inhibition. The largest tumor volume observed in the present study was 1045.3 mm^3 in the PBS control group. The largest tumor length was 15.59 mm and the width was 11.58 mm. However, marked tumor shrinkage was observed in the groups receiving 40 and 100 mg/ml propofol treatment, indicating a potent antitumor effect.

To gain insights into the underlying mechanisms of propofol-induced tumor suppression, immunohistochemical staining was conducted (Fig. 7D and E). The expression levels of the proapoptotic protein Bax and the apoptosis activator cleaved caspase 3 were significantly upregulated, while the expression levels of the antagonist Bcl-xL were significantly downregulated in the 40 and 100 mg/ml propofol treatment groups. Furthermore, the downregulation of the cell cycle marker CCNE2 indicated propofol-induced cell cycle arrest, further contributing to the anti-proliferative effects.

Considering the promising effects observed on 4T1 cell migration and invasion *in vitro*, as well as the absence of metastatic nodules in major organs following propofol treatment, contrasted with the other groups in which metastatic nodules were detected in the lungs (Fig. S4). The present results indicated that propofol at high concentrations may exert substantial inhibitory effects on tumor metastasis *in vivo*.

Collectively, the present *in vivo* investigations demonstrated that propofol effectively suppressed tumor growth and progression through multiple mechanisms, including

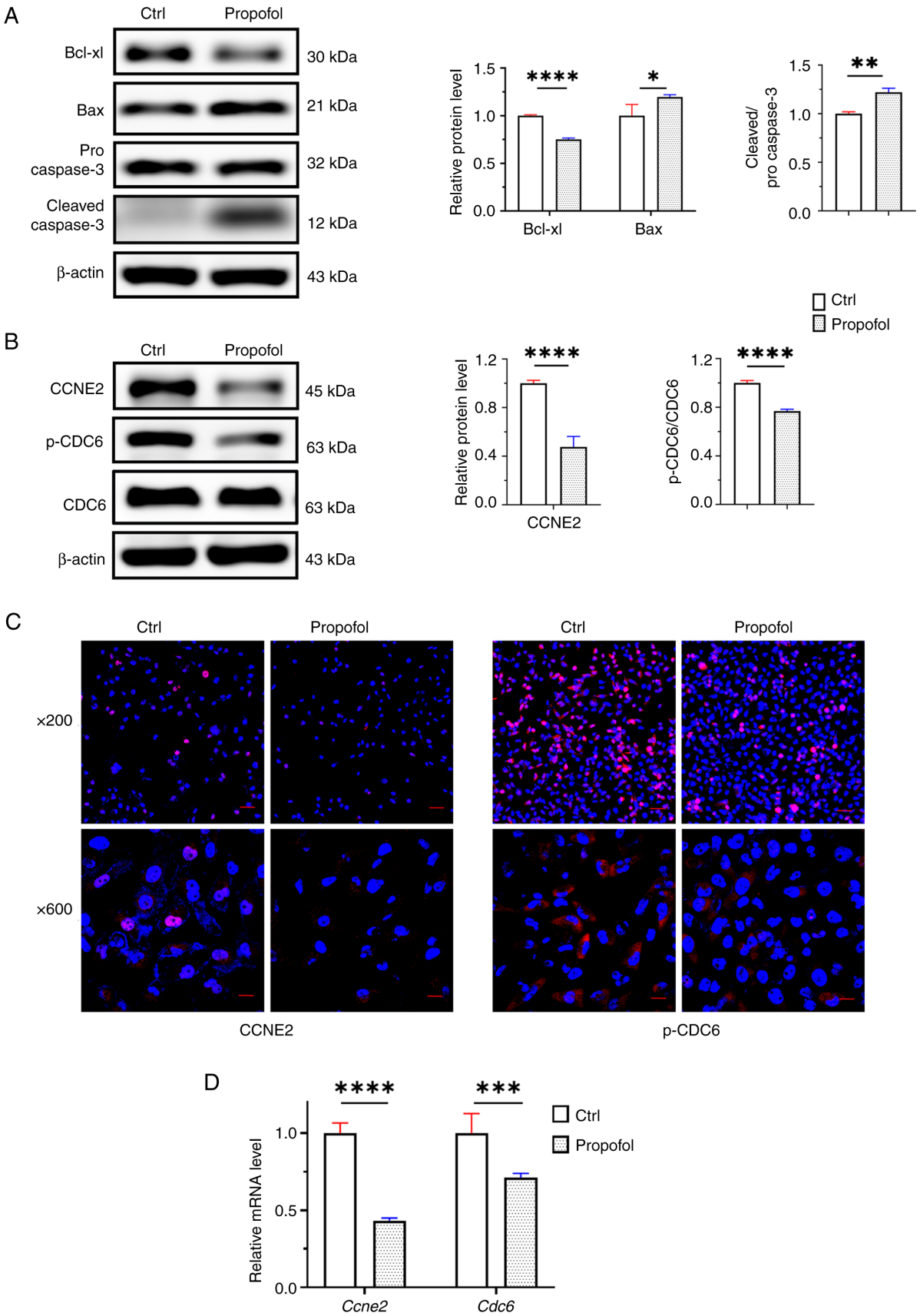

Figure 6. Effects of propofol on the molecular markers of cell apoptosis and cell cycle progression in 4T1 cells. (A) The protein expression levels of apoptosis antagonist Bcl-xL, apoptosis agonist Bax, and apoptosis activator cleaved caspase 3 were assessed after treatment with 100 μg/ml propofol for 24 h in 4T1 cells. Quantification of the protein levels is presented. (B) The protein expression levels of cell cycle makers CCNE2, p-CDC6 and CDC6 were analyzed in 4T1 cells following treatment with 100 μg/ml propofol for 24 h. Quantification of the protein levels is presented. (C) Immunofluorescence images of CCNE2 and p-CDC6 in 4T1 cells after treatment with 100 μg/ml propofol for 24 h. (D) The relative expression of CCNE2 and CDC6 mRNA in 4T1 cells after treatment with 100 μg/ml propofol for 24 h. Statistical analysis was performed using the Student's t-test. Data are presented as the mean ± SD (n=4). *P<0.05, **P<0.01, ***P<0.001 and ****P<0.0001. ns, no significance; ctrl, control; Bcl-xL, B-cell lymphoma-extra large; CCNE2, cyclin E2; p-CDC6, phosphorylated cell division cycle 6.

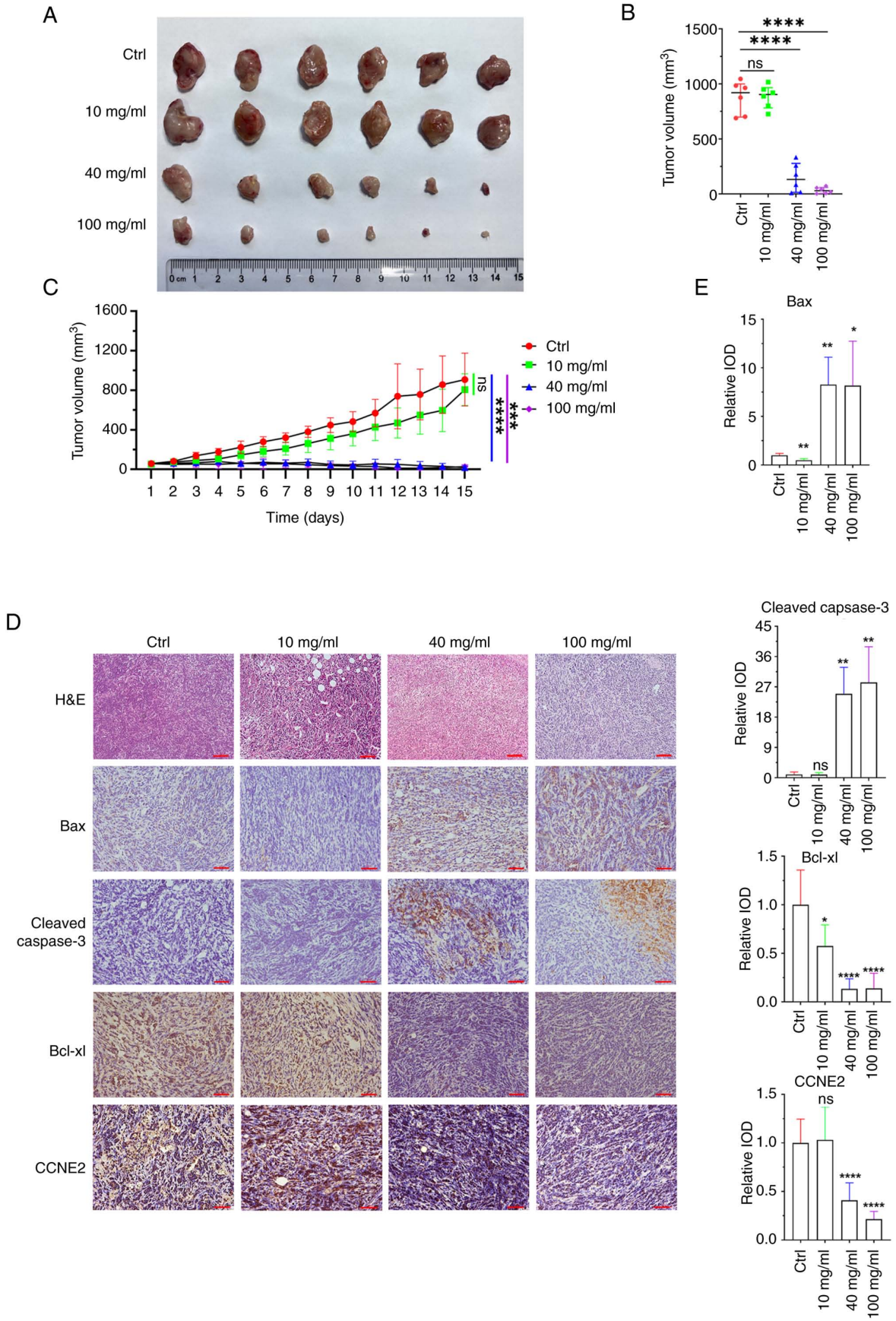

Figure 7. Propofol effectively inhibits the tumor growth *in vivo*. (A) Representative images of tumors from various treatment groups. (B) Dissected tumor volumes at day 15. (C) Tumor volume evolution in each group over the course of treatment. Each point represents the mean tumor volume ± standard error (n=6). (D) H&E staining revealing cell morphology within tumors following various treatments. Immunohistochemical staining depicting the expression of Bax, cleaved caspase 3, Bcl-xL and CCNE2 in tumor cells. Scale bar, 100 μm. (E) Quantitative analysis of the immunohistochemical staining. Statistical analysis was performed using one-way ANOVA with Tukey's post hoc analysis. Data are presented as the mean ± SD. *P<0.05, **P<0.01, ***P<0.001 and ****P<0.0001. ns, no significance; ctrl, control; IOD, integrated optical density; Bcl-xL, B-cell lymphoma-extra large; CCNE2, cyclin E2.

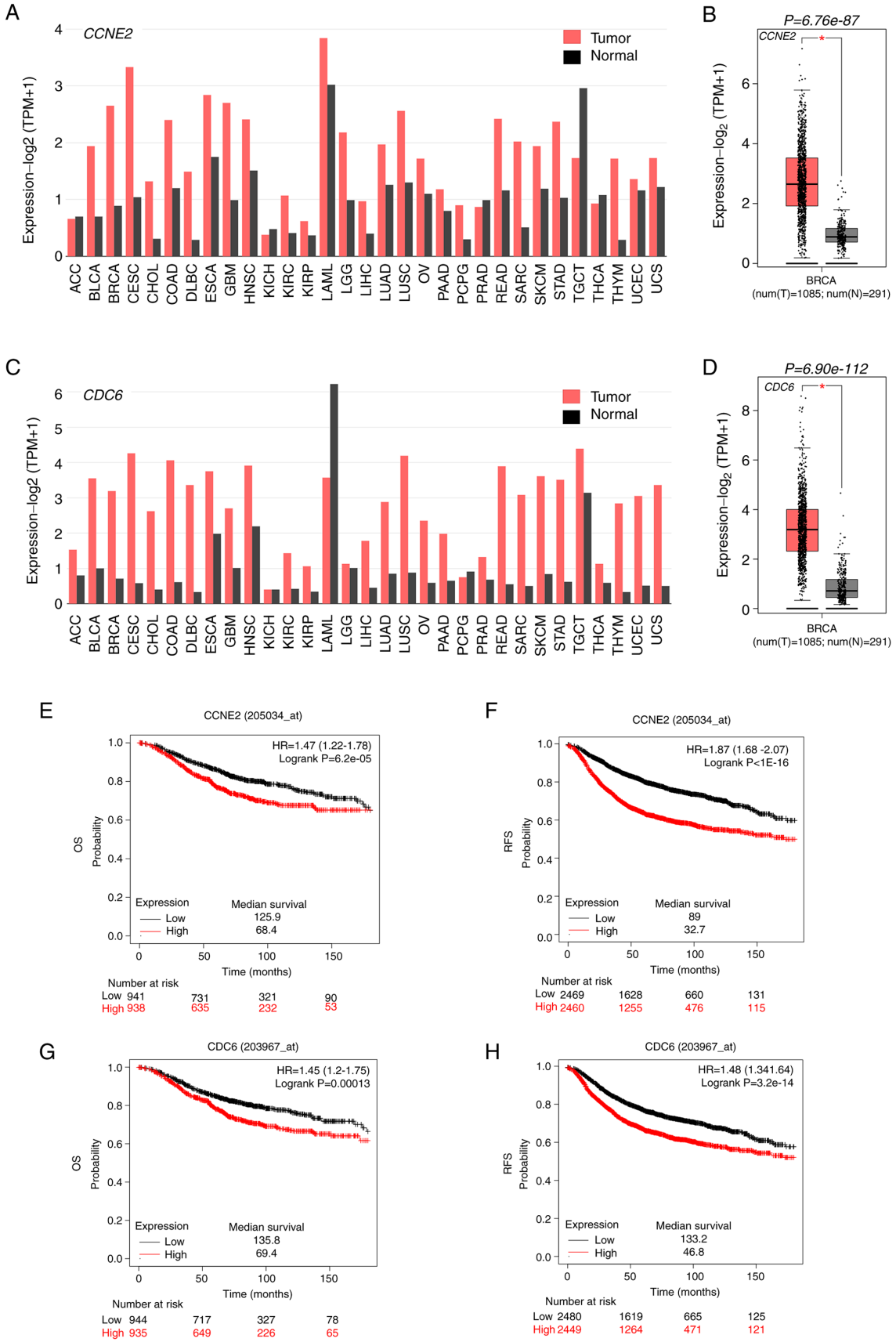

Figure 8. Prognostic implications of CCNE2 and CDC6 expression in breast cancer. (A and B) Expression levels and prognostic value of CCNE2 in various types of human cancers, assessed using the TCGA database. (C and D) Expression levels and prognostic value of CDC6 in various types of human cancers, assessed using the TCGA database. Kaplan-Meier analysis of (E) OS and (F) RFS in patients with breast cancer based on different CCNE2 expression levels from TCGA database, conducted using Kaplan-Meier plotter. Kaplan-Meier analysis of (G) OS and (H) RFS in patients with breast cancer based on different CDC6 expression levels from TCGA database, conducted using Kaplan-Meier plotter. Statistical analysis was performed using the Student's t-test. P-values are displayed, and P<0.05 was considered statistically significant. CCNE2, cyclin E2; CDC6, cell division cycle 6; OS, overall survival; RFS, recurrence-free survival; TCGA, The Cancer Genome Atlas.

promoting tumor cell apoptosis, inducing cell cycle arrest and inhibiting tumor metastasis. These findings strengthen the rationale for its potential as an innovative and promising therapeutic agent for breast cancer treatment, warranting further exploration and consideration for clinical translation.

CCNE2 and CDC6 predict poor outcome and survival in breast cancer. Specifically, increased expression of CCNE2 has been associated with uncontrolled cell proliferation and poor prognosis in cancer patients. Conversely, reduced CCNE2 expression has been linked to cell cycle arrest and apoptosis, underscoring its potential as a promising therapeutic target for cancer treatment (36). On the other hand, CDC6 serves a crucial role in the assembly of the pre-replication complex, essential for licensing DNA for replication. During the G_1 phase, CDC6 facilitates the recruitment of other replication factors to the origin of replication on DNA, ensuring accurate and timely DNA replication during the S phase (37). Dysregulation of CDC6 can lead to aberrant DNA replication and genome instability, contributing to the development of cancer (38).

The upregulation of CCNE2 and CDC6 has been reported in various cancer types, highlighting their critical roles in tumorigenesis and cancer progression (Fig. 8A and C). The present study further investigated the clinical relevance of CCNE2 and CDC6 expression in breast cancer progression. Through analysis of clinical breast cancer samples from The Cancer Genome Atlas database, markedly higher CCNE2 and CDC6 expression was observed in breast cancer tissues compared with normal tissues (Fig. 8B and D). A comprehensive analysis of OS and RFS of patients with breast cancer with varying levels of CCNE2 and CDC6 expression was conducted (Fig. 8E-H). Patients with low CCNE2 and CDC6 expression exhibited significantly improved OS and RFS compared with those with high CCNE2 and CDC6 expression, emphasizing CCNE2 and CDC6 as potential prognostic markers for breast cancer outcomes. The discovery of propofol-mediated downregulation of CCNE2 and CDC6 suggests its potential role in suppressing tumor growth. However, the precise signaling pathway cascade underlying this effect requires further investigation in future studies. Understanding the molecular mechanisms through which propofol modulates CCNE2 and CDC6 expression may unlock novel therapeutic opportunities and facilitate the development of targeted approaches in breast cancer treatment.

Discussion

Breast cancer remains a significant global health concern, necessitating the exploration of novel and effective therapeutic strategies, particularly for triple-negative breast cancer (5,6). Propofol, a well-known intravenous anesthetic in surgical settings, has recently emerged as a promising candidate for breast cancer therapy due to its remarkable antitumor effects, which have been demonstrated both *in vitro* and *in vivo* (26). The multifaceted anticancer properties of propofol, including inhibition of tumor growth, induction of tumor cell apoptosis, cell cycle arrest and suppression of tumor metastasis, have garnered attention from the scientific community (39). Furthermore, its excellent biocompatibility *in vivo* further bolsters its appeal as a safe and well-tolerated treatment option, paving the way for its potential integration into existing breast cancer treatment protocols (40,41).

The investigation into the inhibitory effects of propofol on breast cancer commenced with *in vitro* cell experiments, which unequivocally demonstrated significant suppression of breast cancer cell proliferation, migration and invasion, without impacts on the activity of HUVECs. HUVECs possess well-characterized properties and established culturing protocols. Choosing HUVECs as a control line ensure consistency with existing literature and facilitate comparisons with different studies (42-44). Furthermore, *in vivo* animal models validated these findings, showcasing the impressive ability of propofol to markedly inhibit tumor growth in mice bearing 4T1 tumors. The observed tumor shrinkage was accompanied by visible apoptotic phenotypes in pathological tissue sections, signifying enhanced cell contraction and altered nuclear morphology. Transcriptome sequencing revealed intriguing insights into the molecular mechanisms underlying its antitumor effects. Specifically, propofol treatment upregulated the expression levels of apoptosis-related genes, including the pro-apoptotic protein Bax and the apoptosis activator cleaved caspase 3, while downregulating the expression levels of the antagonist Bcl-xL. These findings indicated that propofol exerted its tumor-suppressive role through the activation of endogenous apoptosis pathways.

Of particular interest were the findings related to the cell cycle regulators, CCNE2 and p-CDC6. Dysregulation of these proteins has been implicated in cancer progression, making them attractive targets for potential cancer therapies (45-47). The downregulation of CCNE2 by propofol led to the arrest of the G_1/S phase transition in breast cancer cells, further corroborating its ability to halt tumor cell proliferation. Similarly, inhibition of p-CDC6 expression by propofol interfered with proper DNA replication during the G_1 phase, contributing to the suppression of cancer cell proliferation. These discoveries shed light on the intricate molecular mechanisms underlying its inhibitory effects on breast cancer cells.

Propofol exerts sedative-hypnotic effects through chloride transport and γ-aminobutyric acid (GABA) receptors, commonly used for induction and maintenance of general anesthesia due to its rapid onset recovery, and minimal adverse effects (48). Propofol may play a role in the tumor microenvironment in patients undergoing surgery. Previous evidence revealed that patients treated with propofol during radical resection of non-small cell lung cancer exhibited lower serum concentrations of tumor angiogenesis-related factors, such as vascular endothelial growth factor compared with those receiving sevoflurane (49). In patients with breast cancer, serum from propofol-treated individuals prompted more apoptosis in ER-negative breast cancer cells compared with serum from sevoflurane-treated patients (50). Perioperative administration of anesthetic agents stimulated the hypothalamic-pituitary-adrenal axis and sympathetic nervous system (51), leading to systemic elevation of immunosuppressive factors such as catecholamines, prostaglandins and glucocorticoids, resulting in NK cell and cytotoxic T lymphocyte (CTL) suppression (52). In contrast to other intravenous anesthetics, propofol increased CTL activity, decreased pro-inflammatory cytokines, and

inhibited PGE2 functions (53). Furthermore, propofol did not alter Th1/Th2, IL-2/IL-4, or $CD4^+/CD8^+$ T cell ratios, thus mitigating surgery-induced immunosuppression (54). These potential effects of propofol on the cardiovascular system and central nervous system may influence tumor regulation outcomes, necessitating further investigation into the specific mechanisms involved.

Remarkably, propofol holds considerable promise as a transformative approach in breast cancer treatment. Notably, it is an existing medication with a long history of clinical use that may be repurposed for cancer therapy, expediting the development of readily available and effective treatments (41). However, it is essential to elucidate the detailed signaling pathway cascade mediating its effects, which warrants further exploration in future studies. Additionally, its impact on other breast cancer subtypes and its potential combination with existing treatments warrant investigation in translational studies and clinical trials.

The significance of these findings extends beyond breast cancer, as the antitumor and immunomodulatory effects of anesthetics in surgery are increasingly recognized (55,56). Given the urgent need for effective and durable breast cancer treatments, the implications of its inhibitory effects on breast cancer cells hold immense clinical relevance. The integration of propofol into breast cancer treatment protocols holds promise for improving patient outcomes, addressing the challenges of high recurrence rates and postoperative complications. However, further research is necessary to optimize the dosage, duration, administration schedules and routes of administration for maximum efficacy and minimal side effects (57). This endeavor becomes particularly pertinent in light of advancing targeted delivery systems, which hold the potential to offer robust support for the efficacious application of propofol.

In conclusion, propofol exhibited robust antitumor effects in breast cancer, offering promising therapeutic opportunities for improving patient outcomes. The unraveling of its molecular mechanisms provides valuable insights for its integration into breast cancer treatment strategies. As research in this area advances, the potential for propofol to revolutionize breast cancer therapy becomes increasingly evident, driving the field of oncology towards more effective and targeted approaches to combat this formidable disease.

Acknowledgements

Not applicable.

Funding

The present study was supported by 'Science and Technology Program of Guangzhou, China' (grant no. 2024A04J6603).

Availability of data and materials

The data generated in the present study may be requested from the corresponding author. In addition, the data of the original RNA-seq generated in the present study may be found in the BioProject/NCBI under accession number PRJNA1103179 or at the following URL: https://www.ncbi.nlm.nih.gov/bioproject/PRJNA1103179.

Authors' contributions

PS performed data curation and formal analysis, conducted investigation and developed methodology. HH curated data, performed formal analysis and wrote the original draft. JCM curated data, performed formal analysis, developed methodology, and wrote the original draft. BF curated and validated data. YZ curated data and performed formal analysis. GQ provided resources, performed formal analysis and edited the manuscript. WZ conceptualized, supervised the study, provided resources and edited the manuscript. ZKC conceptualized and supervised the study, developed methodology, acquired funding, and wrote, reviewed and edited the manuscript. All authors read and approved the final manuscript. PS and HH confirm the authenticity of all the raw data.

Ethics approval and consent to participate

All cell and animal experimental procedures were performed according to protocols approved by the Institutional Ethics Committee of Southern Medical University (approval no. L2019080; Guangzhou, China).

Patient consent for publication

Not applicable.

Competing interests

The authors declare that they have no competing interests.

References

1. Bray F, Laversanne M, Weiderpass E and Soerjomataram I: The ever-increasing importance of cancer as a leading cause of premature death worldwide. Cancer 127: 3029-3030, 2021.
2. Sung H, Ferlay J, Siegel RL, Laversanne M, Soerjomataram I, Jemal A and Bray F: Global cancer statistics 2020: GLOBOCAN estimates of incidence and mortality worldwide for 36 cancers in 185 countries. CA Cancer J Clin 71: 209-249, 2021.
3. Harbeck N and Gnant M: Breast cancer. Lancet 389: 1134-1150, 2017.
4. Waks AG and Winer EP: Breast cancer treatment. JAMA 321: 316, 2019.
5. Bianchini G, De Angelis C, Licata L and Gianni L: Treatment landscape of triple-negative breast cancer-expanded options, evolving needs. Nat Rev Clin Oncol 19: 91-113, 2022.
6. Derakhshan F and Reis-Filho JS: Pathogenesis of triple-negative breast cancer. Annu Rev Pathol 17: 181-204, 2022.
7. Yu M, Pan H, Che N, Li L, Wang C, Wang Y, Ma G, Qian M, Liu J, Zheng M, *et al*: Microwave ablation of primary breast cancer inhibits metastatic progression in model mice via activation of natural killer cells. Cell Mol Immunol 18: 2153-2164, 2021.
8. Kerr AJ, Dodwell D, McGale P, Holt F, Duane F, Mannu G, Darby SC and Taylor CW: Adjuvant and neoadjuvant breast cancer treatments: A systematic review of their effects on mortality. Cancer Treat Rev 105: 102375, 2022.
9. Loibl S, Poortmans P, Morrow M, Denkert C and Curigliano G: Breast cancer. Lancet 397: 1750-1769, 2021.
10. Gradishar WJ, Anderson BO, Abraham J, Aft R, Agnese D, Allison KH, Blair SL, Burstein HJ, Dang C, Elias AD, *et al*: Breast cancer, version 3.2020, NCCN clinical practice guidelines in oncology. J Natl Compr Canc Netw 18: 452-478, 2020.
11. Winkler F, Venkatesh HS, Amit M, Batchelor T, Demir IE, Deneen B, Gutmann DH, Hervey-Jumper S, Kuner T, Mabbott D, *et al*: Cancer neuroscience: State of the field, emerging directions. Cell 186: 1689-1707, 2023.
12. Tohme S, Simmons RL and Tsung A: Surgery for cancer: A trigger for metastases. Cancer Res 77: 1548-1552, 2017.

13. Badwe RA, Parmar V, Nair N, Joshi S, Hawaldar R, Pawar S, Kadayaprath G, Borthakur BB, Rao Thammineedi S, Pandya S, *et al*: Effect of peritumoral infiltration of local anesthetic before surgery on survival in early breast cancer. J Clin Oncol 41: 3318-3328, 2023.
14. Sessler DI, Pei L, Huang Y, Fleischmann E, Marhofer P, Kurz A, Mayers DB, Meyer-Treschan TA, Grady M, Tan EY, *et al*: Recurrence of breast cancer after regional or general anaesthesia: A randomised controlled trial. Lancet 394: 1807-1815, 2019.
15. Zhong L, Li Y, Xiong L, Wang W, Wu M, Yuan T, Yang W, Tian C, Miao Z, Wang T and Yang S: Small molecules in targeted cancer therapy: Advances, challenges, and future perspectives. Signal Transduct Target Ther 6: 201, 2021.
16. Jin MZ and Jin WL: The updated landscape of tumor microenvironment and drug repurposing. Signal Transduct Target Ther 5: 166, 2020.
17. Sinha D, Sarkar N, Biswas J and Bishayee A: Resveratrol for breast cancer prevention and therapy: Preclinical evidence and molecular mechanisms. Semin Cancer Biol 40-41: 209-232, 2016.
18. Gong F, Ma JC, Jia J, Li FZ, Wu JL, Wang S, Teng X and Cui ZK: Synergistic effect of the anti-PD-1 antibody with blood stable and reduction sensitive curcumin micelles on colon cancer. Drug Deliv 28: 930-942, 2021.
19. Hu C, Iwasaki M, Liu Z, Wang B, Li X, Lin H, Li J, Li JV, Lian Q and Ma D: Lung but not brain cancer cell malignancy inhibited by commonly used anesthetic propofol during surgery: Implication of reducing cancer recurrence risk. J Adv Res 31: 1-12, 2021.
20. Su Z, Liu HL, Qi B and Liu Y: Effects of propofol on proliferation and apoptosis of cardia cancer cells via MAPK/ERK signaling pathway. Eur Rev Med Pharmacol Sci 24: 428-433, 2020.
21. Peng Z and Zhang Y: Propofol inhibits proliferation and accelerates apoptosis of human gastric cancer cells by regulation of microRNA-451 and MMP-2 expression. Genet Mol Res 15, 2016.
22. Du Q, Zhang X, Zhang X, Wei M, Xu H and Wang S: Propofol inhibits proliferation and epithelial-mesenchymal transition of MCF-7 cells by suppressing miR-21 expression. Artif Cells Nanomed Biotechnol 47: 1265-1271, 2019.
23. Li H, Lu Y, Pang Y, Li M, Cheng X and Chen J: Propofol enhances the cisplatin-induced apoptosis on cervical cancer cells via EGFR/JAK2/STAT3 pathway. Biomed Pharmacother 86: 324-333, 2017.
24. Huang Y, Lei L and Liu Y: Propofol improves sensitivity of lung cancer cells to cisplatin and its mechanism. Med Sci Monit 26: e919786, 2020.
25. Gao Y, Zhou Y, Wang C, Sample KM, Yu X and Ben-David Y: Propofol mediates pancreatic cancer cell activity through the repression of ADAM8 via SP1. Oncol Rep 46: 249, 2021.
26. Fang P, Zhou J, Xia Z, Lu Y and Liu X: Effects of propofol versus sevoflurane on postoperative breast cancer prognosis: A narrative review. Front Oncol 11: 793093, 2021.
27. Oh CS, Hong SW, Park S, Kwon Y and Kim SH: Effect of equipotent doses of propofol and sevoflurane on endoplasmic reticulum stress during breast cancer surgery. Korean J Anesthesiol 75: 487-495, 2022.
28. Li R, Liu H, Dilger JP and Lin J: Effect of propofol on breast cancer cell, the immune system, and patient outcome. BMC Anesthesiol 18: 77, 2018.
29. Li J, Liu M, Zeng B and Wang Z: Propofol induces hepatocellular carcinoma cell apoptosis via regulating miR-105/JAK2/STAT3 axis. Cytokine 148: 155649, 2021.
30. Li Z, Liu H, Zhang Y and Tan H: The effect of propofol on the proliferation and apoptosis of hepatocellular carcinoma cells through TGF-B1/Smad2 signaling pathway. Bioengineered 12: 4581-4592, 2021.
31. Zhang L, Wang N, Zhou S, Ye W, Jing G and Zhang M: Propofol induces proliferation and invasion of gallbladder cancer cells through activation of Nrf2. J Exp Clin Cancer Res 31: 66, 2012.
32. Liu Q, Sheng Z, Cheng C, Zheng H, Lanuti M, Liu R, Wang P, Shen Y and Xie Z: Anesthetic propofol promotes tumor metastasis in lungs via GABA(A) R-dependent TRIM21 modulation of Src expression. Adv Sci (Weinh) 8: e2102079, 2021.
33. Livak KJ and Schmittgen TD: Analysis of relative gene expression data using real-time quantitative PCR and the 2(-Delta Delta C(T)) method. Methods 25: 402-408, 2001.
34. Monteran L, Ershaid N, Doron H, Zait Y, Scharff Y, Ben-Yosef S, Avivi C, Barshack I, Sonnenblick A and Erez N: Chemotherapy-induced complement signaling modulates immunosuppression and metastatic relapse in breast cancer. Nat Commun 13: 5797, 2022.
35. Dong J, Zhu C, Zhang F, Zhou Z and Sun M: 'Attractive/adhesion force' dual-regulatory nanogels capable of CXCR4 antagonism and autophagy inhibition for the treatment of metastatic breast cancer. J Control Release 341: 892-903, 2022.
36. Yang J, Dong Z, Ren A, Fu G, Zhang K, Li C, Wang X and Cui H: Antibiotic tigecycline inhibits cell proliferation, migration and invasion via down-regulating CCNE2 in pancreatic ductal adenocarcinoma. J Cell Mol Med 24: 4245-4260, 2020.
37. Speck C, Chen Z, Li H and Stillman B: ATPase-dependent cooperative binding of ORC and Cdc6 to origin DNA. Nat Struct Mol Biol 12: 965-971, 2005.
38. Lim N and Townsend PA: Cdc6 as a novel target in cancer: Oncogenic potential, senescence and subcellular localisation. Int J Cancer 147: 1528-1534, 2020.
39. Wu KC, Liao KS, Yeh LR and Wang YK: Drug repurposing: The mechanisms and signaling pathways of anti-cancer effects of anesthetics. Biomedicines 10: 1589, 2022.
40. Skues MA and Prys-Roberts C: The pharmacology of propofol. J Clin Anesth 1: 387-400, 1989.
41. Walsh CT: Propofol: Milk of Amnesia. Cell 175: 10-13, 2018.
42. Shashni B, Nishikawa Y and Nagasaki Y: Management of tumor growth and angiogenesis in triple-negative breast cancer by using redox nanoparticles. Biomaterials 269: 120645, 2021.
43. Yang Q, Chen Z, Qiu Y, Huang W, Wang T, Song L, Sun X, Li C, Xu X and Kang L: Theranostic role of (89)Zr- and (177) Lu-labeled aflibercept in breast cancer. Eur J Nucl Med Mol Imaging 51: 1246-1260, 2024.
44. Alboabdullah AKA, Goodarzi MT and Homayouni Tabrizi M: The Lawson-loaded β-cyclodextrin nanocarriers (LB-NCs) a novel targeted cancer cell in stomach and breast cancer as a drug delivery system. Naunyn Schmiedebergs Arch Pharmacol: Mar 14, 2024 (Epub ahead of print).
45. Mailand N and Diffley JFX: CDKs promote DNA replication origin licensing in human cells by protecting Cdc6 from APC/C-dependent proteolysis. Cell 122: 915-926, 2005.
46. Sieuwerts AM, Look MP, Meijer-van Gelder ME, Timmermans M, Trapman AMAC, Garcia RR, Arnold M, Goedheer AJW, de Weerd V, Portengen H, *et al*: Which cyclin E prevails as prognostic marker for breast cancer? Results from a retrospective study involving 635 lymph node-negative breast cancer patients. Clin Cancer Res 12: 3319-3328, 2006.
47. Bömer M, Pérez-Salamó I, Florance HV, Salmon D, Dudenhoffer JH, Finch P, Cinar A, Smirnoff N, Harvey A and Devoto A: Jasmonates induce Arabidopsis bioactivities selectively inhibiting the growth of breast cancer cells through CDC6 and mTOR. New Phytol 229: 2120-2134, 2021.
48. Feng C, Qian D and Chen C: A meta-analysis and systematic review of propofol on liver ischemia-reperfusion injury protection during hepatocellular carcinoma anesthesia surgery. Ann Palliat Med 10: 6726-6735, 2021.
49. Sen Y, Xiyang H and Yu H: Effect of thoracic paraspinal block-propofol intravenous general anesthesia on VEGF and TGF-β in patients receiving radical resection of lung cancer. Medicine (Baltimore) 98: e18088, 2019.
50. Jaura AI, Flood G, Gallagher HC and Buggy DJ: Differential effects of serum from patients administered distinct anaesthetic techniques on apoptosis in breast cancer cells in vitro: A pilot study. Br J Anaesth 113 (Suppl 1): i63-i67, 2014.
51. Kim R: Anesthetic technique and cancer recurrence in oncologic surgery: Unraveling the puzzle. Cancer Metastasis Rev 36: 159-177, 2017.
52. Greenfeld K, Avraham R, Benish M, Goldfarb Y, Rosenne E, Shapira Y, Rudich T and Ben-Eliyahu S: Immune suppression while awaiting surgery and following it: Dissociations between plasma cytokine levels, their induced production, and NK cell cytotoxicity. Brain Behav Immun 21: 503-513, 2007.
53. Kushida A, Inada T and Shingu K: Enhancement of antitumor immunity after propofol treatment in mice. Immunopharmacol Immunotoxicol 29: 477-486, 2007.
54. Inada T, Yamanouchi Y, Jomura S, Sakamoto S, Takahashi M, Kambara T and Shingu K: Effect of propofol and isoflurane anaesthesia on the immune response to surgery. Anaesthesia 59: 954-959, 2004.
55. Yap A, Lopez-Olivo MA, Dubowitz J, Hiller J and Riedel B; Global Onco-Anesthesia Research Collaboration Group: Anesthetic technique and cancer outcomes: A meta-analysis of total intravenous versus volatile anesthesia. Can J Anaesth 66: 546-561, 2019.
56. Kim R: Effects of surgery and anesthetic choice on immunosuppression and cancer recurrence. J Transl Med 16: 8, 2018.
57. Korn EL, Moscow JA and Freidlin B: Dose optimization during drug development: Whether and when to optimize. J Natl Cancer Inst 115: 492-497, 2023.